J. Fluid Mech. (2002), *vol.* 457, *pp.* 157–180.
DOI: 10.1017/S002211200200784X Printed in the United Kingdom

Experiments on the stability of sinusoidal flow over a circular cylinder

By TURGUT SARPKAYA

Mechanical Engineering, Naval Postgraduate School, Monterey, CA 93943, USA

(Received 10 July 2001 and in revised form 29 October 2001)

The instabilities in a sinusoidally oscillating non-separated flow over smooth circular cylinders in the range of Keulegan–Carpenter numbers, K, from about 0.02 to 1 and Stokes numbers, β, from about 10^3 to 1.4×10^6 have been observed from inception to chaos using several high-speed imagers and laser-induced fluorescence. The instabilities ranged from small quasi-coherent structures, as in Stokes flow over a flat wall (Sarpkaya 1993), to three-dimensional spanwise perturbations because of the centrifugal forces induced by the curvature of the boundary layer (Taylor–Görtler instability). These gave rise to streamwise-oriented counter-rotating vortices or mushroom-shaped coherent structures as K approached the K_h values theoretically predicted by Hall (1984). Further increases in K for a given β led first to complex interactions between the coherent structures and then to chaotic motion. The mapping of the observations led to the delineation of four states of flow in the (K, β)-plane: stable, marginal, unstable, and chaotic.

1. Introduction

Sinusoidally oscillating flow about a circular cylinder or the sinusoidal motion of a cylinder in a viscous fluid otherwise at rest is of practical as well as fundamental importance because of its relevance to the design of structures in the marine environment (Sarpkaya 1976, 1986), to the understanding of beach processes and bed ripples (Lyne 1971; Hara & Mei 1990*a*, *b*; Scandura, Vittorio & Blondeaux 2000 and references therein), and to the quantification of g-jitter effects on crystal growth and natural convection in microgravity environment (Volfson & Vinals 2001 and references therein). It appears that the numerical simulation of the more realistic three-dimensional flows encountered in practical applications is beyond the power of present computers.

The experiments described herein deal more specifically with the classical problem of Schlichting (1932, 1979) who has shown that the oscillatory motion of a cylinder induces a steady secondary flow outside the boundary layer, and presents typical patterns of such a flow. Subsequently, Batchelor (1967) and Gershuni & Lybimov (1988) arrived at similar conclusions. It is well known that in a sinusoidally oscillating flow over a smooth circular cylinder the structure of the flow depends primarily on the Keulegan–Carpenter number $K = 2\pi A/D$, where A is the amplitude of the relative motion and D is the cylinder diameter, and the Stokes number $\beta = fD^2/\nu$, where f is the frequency of flow (or cylinder) oscillation and ν the kinematic viscosity of the fluid.

The first experiments of particular relevance to this paper were conducted by Honji (1981) in the range of Stokes numbers from 68.8 to 700. He visualized the flow around

a transversely oscillating cylinder in a fluid otherwise at rest and observed, in a plane normal to the direction of cylinder motion, that mushroom-shaped vortices arrange themselves alternately in a vertical double row, i.e. along the crowns of the cylinder where the local ambient velocity is maximum. These vortices are then convected along the direction of oscillation to create equally spaced 'integrated streak sheets' with their contra-rotating vortices. Sarpkaya (1986) extended the range of observations to higher β values (about 5500). Tatsuno & Bearman (1990) made a visual study of the oscillatory flow in the range $1.6 < K < 15$ and $5 < \beta < 160$. The present experiments were conducted at β values two to three orders of magnitude larger than those of Honji using considerably larger cylinders, facilities, and frequencies of oscillation.

Hall (1984) carried out a stability analysis of the unsteady attached boundary layer on a cylinder oscillating transversely in a viscous fluid in both linear and weakly nonlinear regimes. In order to simplify the problem, Hall assumed that the oscillation frequency is large. This reduced the basic stability problem (dependent upon two spatial coordinates and time) to a system dependent only on a radial variable and time. Then the primary objective of the analysis became the determination of the parameter range in which the two-dimensional solution is a stable solution of the Navier–Stokes equations. This led to the K_h–β relationship given by

$$K_h = 5.78\beta^{-1/4}(1 + 0.21\beta^{-1/4} + \cdots), \tag{1.1}$$

where $K_h(\beta)$ will be called the 'Hall line'. It represents a marginal condition between a featureless two-dimensional flow and an unstable region (vortex interactions, turbulence and separation). It does not represent a critical line, say K_{cr}, between a region of absolute stability and the growth of three-dimensional instabilities leading to mushroom-shaped structures. As noted by Hara & Mei (1990*a*), $K_h\beta^{1/4} = 5.78$, represents, as a first approximation to equation (1.1), the fact that an instability of centrifugal type can occur on a two-dimensional flow when the Taylor number ($Ta = A^2/D\delta \equiv K\beta^{1/4}$) exceeds a certain threshold where $\delta = (\nu/\omega)^{1/2}$ is proportional to the viscous boundary layer thickness and $\omega\,(= 2\pi f)$ is the angular frequency. The inception of instabilities in a three-dimensional periodic flow due to the presence of streamwise vorticity (as in Taylor–Görtler vortices) has not yet been investigated analytically or experimentally.

The fairly regular mushroom-shaped structures observed by Honji were named the 'Honji instability' by Sarpkaya (1986). They will now be renamed either the 'Honji-type coherent structures' or 'mushroom-shaped structures' or, simply, 'coherent structures, CS', in preparation for the discussion of irregular or transitional 'quasi-coherent structures, QCS' occurring over a finite region of K values, extending from a critical value of K_{cr} to K_h, and culminating in nearly uniform mushroom-shaped structures. With a small increase in K, the vortices begin to interact with each other and the flow transitions into turbulence, with no apparent periodicity along the crown of the cylinder. Thus, equation (1.1) represents a narrow band in which the mushroom-shaped coherent structures reach their ultimate strength and uniformity along the crown of the cylinder as evidenced by the fact that (1.1) is entirely consistent with the experiments of Honji (1981) within the range of comparison ($68.8 < \beta < 700$). The structures in the region $K > K_h$ will be discussed later.

The purpose of the present paper is to observe the instabilities in a sinusoidally oscillating non-separated flow past smooth circular cylinders in the range of Keulegan–Carpenter numbers from about 0.02 to 1 and Stokes numbers from about 10^3 to 1.4×10^6. The boundary layer structures have been examined by means of laser-induced fluorescence. First, the behaviour of the most representative coherent struc-

tures near Hall's (1984) theoretical prediction (i.e. at $K \approx K_h$) are presented. Then, the inception of instabilities near the critical K_{cr} and the evolution of QCS resembling incomplete mushrooms in the range $K_{cr} < K < K_h$ are discussed. Finally, for $K > K_h$ the mutual interaction of the neighbouring mushrooms and the onset of chaotic motion are described in as much detail as possible through the use of representative still photographs. These are followed by the delineation of the stable, marginal, unstable and chaotic regions of flow in the (K, β)-plane with the hope that direct numerical simulations by means of Navier–Stokes and continuity equations will not only confirm them but also provide additional details on those flow features which cannot yet be measured or visualized.

2. Experimental apparatus and procedures

The primary goals for the equipment were to achieve a relatively large β in non-separated sinusoidally oscillating flow relative to circular cylinders in the range $0.02 < K < 1$ and to use flow visualization to delineate the inception and evolution of flow structures in the boundary layer.

The experiments were conducted in three different facilities: a U-shaped water tunnel where the flow oscillated about cylinders at a constant frequency, in a rectangular basin where the test cylinder was subjected to forced oscillations at desired frequencies, and in a larger reservoir where the horizontally mounted test cylinders were suspended between two (sufficiently large) end plates of a vertical pendulum and subjected to resonant forced oscillations. The features common to all three facilities are summarized at the end of the description of the third facility.

The working section of the U-shaped water tunnel is 145 cm high, 92 cm wide, and 10.7 m long. The two 6.7 m vertical sections are 183 cm by 92 cm each. The oscillatory flow in the tunnel is driven by a computer-controlled pneumatic system. The spectra of the velocity at various positions in the test section (obtained through the use of a three-dimensional LDV system) have confirmed that the contributions of the second and higher harmonics are negligible. The transient period to reach a constant K from rest varied from six to ten cycles for $K < 1$, with the fluid oscillating at its resonant frequency of $f = 0.187$ Hz. This tunnel is used for cylinders with $D < 170$ mm. Additional details of the design and operation of the tunnel are given elsewhere (Sarpkaya 1976, 1977).

Normally, the amplitude of oscillations and hence the Keulegan–Carpenter number are changed from one value to another by enlarging or constricting a two-dimensional orifice in the pneumatic system. For the present experiments, however, a particular Keulegan–Carpenter number was set up in the tunnel either by gradually increasing the prevailing K or by starting the flow from rest (after a period of about an hour). The reasons for the two flow-establishment schemes were partly to explore the history effects on the evolution of the flow structures and partly to replenish the fluorescent dye which dissolves after many cycles of oscillation. Extensive observations and tape recordings with both schemes have shown that the instabilities did not develop immediately after arriving at a new K value but took about 10 cycles to reach a quasi-steady state. The incipient structure and subsequent evolution of the resulting instabilities were so similar that an independent observer could not have deduced from observations and viewing of the video tapes how the new flow state was created, i.e. no history affects were observed.

The second facility is a 4.6 m long, 92 cm wide, and 183 cm high rectangular basin. The test cylinders ($D < 260$ mm) were subjected to forced oscillations at desired

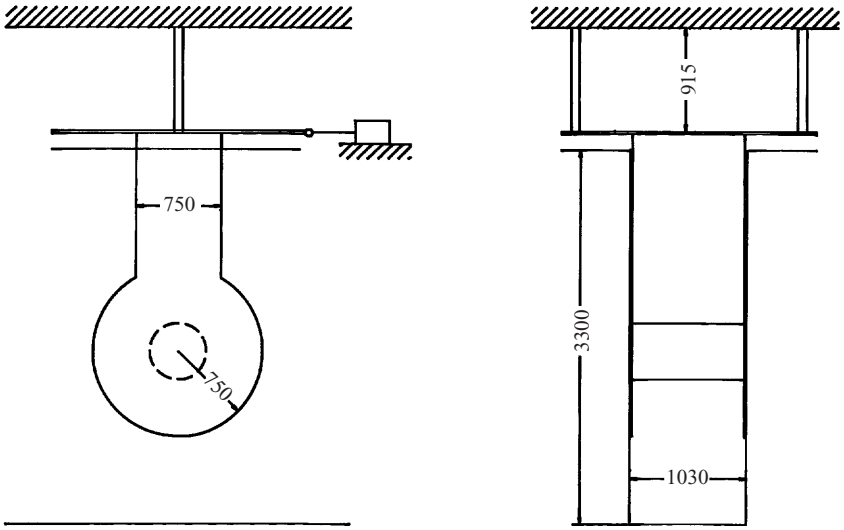

FIGURE 1. The third facility: a schematic drawing of the oscillating pendulum (all dimensions are in mm).

frequencies ($f < 4$ Hz) using a simple scotch yoke mechanism mounted rigidly on top of the basin. The cylinders (909 mm long) were rigidly attached to streamlined circular side plates of diameter $2.5D$. The maximum amplitude of oscillation was kept smaller than 25 mm.

The third facility (figure 1) is very similar to the second one, except for its size. It is a 330 cm deep, 103 cm wide, and 457 cm long tank with several removable tempered-glass windows (at the cylinder level), large enough for viewing and photographing. The pendulum was made of two streamlined side plates. The lower circular parts of each side plate also served as end plates for the cylinders as in the second facility. The top of each plate was welded to a 25 mm thick steel plate, 14 cm above the water level. Then, two wide-flange I-beams (91.5 cm long) were bolted to the top of the 25 mm metal plate and to the support structure above. The I-beams were changed as needed to achieve the desired natural frequency and the oscillation amplitude (at the cylinder axis) in water.

The test cylinders (20 cm $< D <$ 50 cm, with $L = 1018$ mm) were subjected to forced oscillations through the use of a scotch yoke and servo-controlled motor, connected to the pendulum at the level of the 25 mm steel plate. An LDV (a linear differential displacement transducer) and an accelerometer were attached to the pendulum at the cylinder level (160 cm above the tank bottom). The spectrum of the accelerations show single peaks with no secondary frequencies for $f < 6$ Hz and $A < 40$ mm.

One half of the 14 cm space between the water surface and the steel plate was used to mount a small vertical tube of about 20 cm long as housing for the lenses and the head of the fibre-optic cable. Its top end (7 cm below the steel plate) was open and the bottom end (covered and sealed with a circular Plexiglas sheet) pierced the water surface (about 13 cm) through the Plexiglas cover on top of the reservoir. It was constructed such that it can be moved along a line in the mid-plane normal to the axis of the test cylinder and tilted up to $\pm 10°$. The cylinders were rigidly attached to the end plates (the pendulum) to minimize the interference effects. A clearance of about 12 mm was provided between an end plate and the tank wall.

Pluck tests (subjecting a body to damped oscillations by releasing it from an

initially displaced position) were not used. The reason for this is primarily that the larger the cylinder the longer the time (the number of cycles of oscillation) taken for the establishment of the mushroom-shaped structures. Cylinders subjected to pluck tests did not always accord the opportunity for sufficiently long observations and recording at a given K. The rapidly decaying transient motions have transformed them into irregular vortical forms.

The most important common features of the facilities were as follows. A cross-flow micro-filtration and de-aeration system was used to remove any suspended fine particles from the water after it was discovered that the presence of small air bubbles and the attachment of some of them to the cylinder surface could interfere with or alter the character of the coherent or quasi-coherent structures. The filtration system was turned off during the experiments.

All cylinders were made absolutely airtight and neutrally buoyant when submerged. They were painted matte black and polished carefully with velvet. The thickness of the dye layer, determined from the dye volume introduced and the area it spread on the cylinder, was about 0.4 mm. In the second and third facilities the top of the water surface was covered with Plexiglas plates of about 12 mm thick (25 mm below the free surface) with appropriate size openings for the suspension mechanisms, to prevent free-surface waves from developing and affecting the visualizations while model is oscillating.

Two types of laser light sheets were used. The first was a portable laser sheet system, similar to that proposed by Koga, Abrahamson & Eaton (1987). It was set up to create a thin sheet of nearly collimated continuous light which can be positioned at any desired angle relative to the cylinder or the ambient flow as shown in Sarpkaya (1993). The thickness of the light sheet was varied from about 1.5 mm to 2 mm. It was used for relatively small frequencies of flow oscillation. The second light sheet was provided by a Yag laser of a digital particle image velocimeter (DPIV) system, pulsing at 32 ms intervals for periods of 7 ns. This provided an intense light sheet approximately l.5 mm thick, and allowed visualization of flow structures along the crown of the cylinder. A digital video camera (with frame rates from 250 to 8000 frames/s and shutter speeds from 1/60 to 1/10 000 s) was used to record images on memory cards which were subsequently downloaded onto S-VHS tapes.

Normally, the light sheet was placed in a vertical plane passing through the crown and the axis of the cylinder. From time to time, the light sheet was tilted 5° to 10° forward or backward, to one or the other side of the crown, to photograph the counter-rotating streamwise vortices simultaneously with the mushrooms in the glow reflected from the cylinder. Fluorescent dyes (a mixture of water drawn out of the tanks and a small amount of fluorescein or Rhodamine powder, strained several times through a fine cloth) were used primarily because they do not change the viscosity and density of water and their molecular diffusion and miscible dispersion are much higher than that of the 'smoke' produced from a metallic compound through electrolytic precipitation. The dye was introduced along a centrally located 20 cm to 40 cm long section of the cylinder with a rotatable and horizontally retractable, L-shaped, remote arm (a 50 cm long, 3 mm diameter, closed-end tube, with linearly spaced rectangular slots along its length). When the arm was rotated upward and retracted, it rested at the bottom of the Plexiglas cover. When rotated downward, the spacing between the dye tube and the crown of the cylinder was less than 1 mm. Then the dye was deposited on the cylinder with a very small differential hydrostatic pressure between the crown and the external dye reservoir. In a few cycles of oscillation, the dye distributed smoothly and uniformly over a known area and remained there until upward fluid

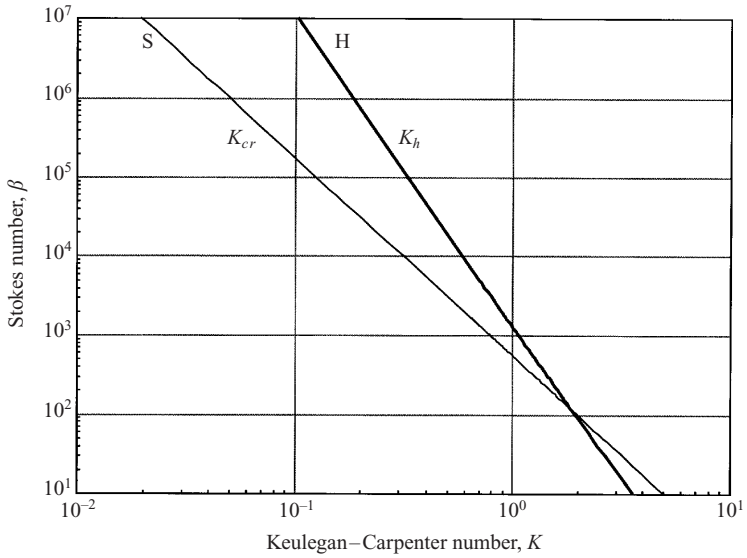

FIGURE 2. Stokes number versus Keulegan–Carpenter number. The line marked S (denoting stability) defines the marginal region. It separates the stable region on the left from the unstable region on the right. The line H (called the Hall line) is given by equation (1.1), after Hall (1984).

motions caused parts of it to lift to show the cross-sections of the instabilities. The evolution of the resulting structures was recorded on video tapes or memory cards, depending on the frequency of oscillation of the flow or the cylinder and the camera used, simultaneously with the instantaneous acceleration of the ambient flow or the amplitude of oscillation of the cylinder.

3. Results and discussion

In preparation for the presentation of the results, the (K, β)-plane was divided (at least initially) into three regions as shown in figure 2. The line labelled H, after Hall (1984), represents equation (1.1). Each K value on the Hall line corresponds to a K_h value at which the mushroom-shaped coherent structures occur. The line marked S (denoting stability) defines the marginal region. It separates the stable region on the left from the unstable region on the right. It will be shown that there is a stable region ($K < K_{cr}$) in which there are no structures identifiable by flow visualization, an unstable transition region ($K_{cr} < K < K_h$) in which there are QCS (quasi-coherent structures) leading to mushroom-shaped coherent structures at $K \approx K_h$, and an increasingly chaotic region ($K > K_h$) where coherent structures undergo complex interactions, eventually leading to separation and turbulence. It must be emphasized that the two boundaries defined by $K = K_{cr}$, (line S) and $K = K_h$ (line H) are not sharp demarcation lines. They should be regarded as narrow fuzzy regions whose extent depends on the observer's ability to interpret 'small disturbances' and nearly 'perfect' mushrooms in laboratory experiments. It should also be noted that the line S is assumed to be straight, whereas line H is not straight, particularly at lower values of β, because of the second and higher terms of equation (1.1).

Sufficient evidence to exemplify the various events in each region in figure 2 is presented in the remainder of the paper and the data obtained in the course of the investigation are plotted in figure 17 (§ 3.2.4).

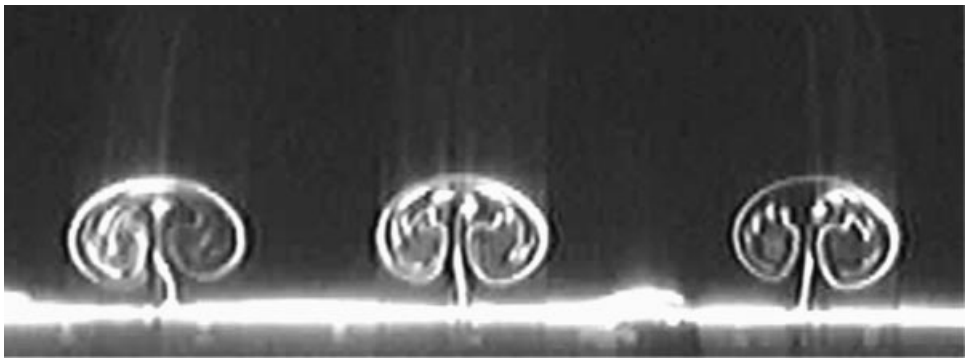

FIGURE 3. A close-up view of three mushrooms and their contra-rotating vortices. The vortex tubes are made visible by tilting the light sheet about 10° to enhance the glow that cylinder reflects back to the vortex tubes. Second facility, $A = 18.4\,\text{mm}$, $D = 200\,\text{mm}$, $f = 0.26\,\text{Hz}$, $K = 0.58$, $\beta = 9956$, $s/D = 0.088$. In this and in all other photographs to follow, the direction of oscillation (flow or cylinder) is perpendicular to the page.

The descriptions to follow are based on extensive video viewing and the information extracted from it in terms of occurrence of various types of structures, mindful of the fact that the vagaries of flow visualization do not always provide correct insight into the actual physics. Furthermore, one can only repeat the complaint registered by practically all experimenters on this subject that still photographs (printed from the digitized frames of the video) do not convey as much information as motion pictures. Furthermore, it will be nearly impossible to provide photographic evidence of the events described for each and every data point. This will amount to reproducing about 800 000 frames that were used in the descriptions to follow. It is also understood that no single realization at a given point in the (K, β)-plane can ever exactly repeat itself. Thus, the figures should be regarded as examples of what might generally happen in the vicinity of a point in the (K, β)-plane.†

The regions and boundaries noted above will be described in the following order: mushroom-shaped coherent structures for $K = K_h$; inception of instabilities, the delineation of $K \approx K_{cr}$, and the evolution of quasi-coherent structures; the interaction of mushrooms and other events for $K > K_h$, leading to chaos and, eventually, to turbulence and separation; and, finally, the quantification of the lines of stability and mushroom spacing. In photographs to be presented, the two-dimensional light sheet is parallel to the page and the cylinder motion is always normal to the page. Individual frames unfortunately lack the very vivid and far more convincing impressions gained from watching the video tapes. Nevertheless, every effort is made to convey some of this dynamic interaction through the use of the most representative succession of photographs during one or more cycles in describing the flow in the (K, β)-plane. The captions of the representative photographs show the most relevant parameters (test facility, A, D, f, K, β, and, whenever applicable, s/D where s is the average mushroom spacing).

3.1. *Mushroom-shaped coherent structures on $K = K_h$ and their evolution*

Figure 3 shows three of a dozen of almost uniformly shaped and spaced mushrooms near the crown of the cylinder ($K = K_h = 0.58$). Each is composed of two, relatively weak, counter-rotating vortices and a stem which appears and disappears periodically

† We hope to make video clips available for viewing on a web site in the near future.

as the neighbouring boundary layers converge and diverge. The leaning of the light sheet backwards (about 5° to 10°) relative to the page enables one to visualize the smoothly integrated dye sheets. The occurrence of the Helmholtz instability on the contra-rotating vortex sheets was not uncommon (see the mushroom on the right). Figure 3 also shows that each mushroom has its own asymmetry with respect to a vertical plane which persists over its lifetime but there is no average directional bias at any spanwise position along the cylinder.

Honji (1981), working with relatively small β values and using the electrolytic precipitation method, observed mushroom vortex chains lying in the tubular sheet. The vortex tubes observed in the present investigation always had fairly smooth surfaces as in figure 3. This may be a consequence of our use of dyes with much higher rates of dispersion at larger β values (see Probstein 1995 for an elegant discussion of radial and axial miscible dispersions).

3.1.1. *How does a mushroom grow and sustain itself?*

Mushrooms on the Hall line (i.e. in an established periodic flow field, characterized by fixed values of K_h and β) come into existence through a number of cycles of incremental growth (near $U = U_m$) and decay (near $U = 0$) (where U is the velocity of the ambient fluid) until they reach mature sizes and quasi-steady states. Then a series of characteristic events help them to sustain themselves. Figure 4(a) shows that the stems of the mushrooms are nearly devoid of dye at $U \approx 0$ and there is no feeding of the boundary layer fluid into the mushrooms. In fact, at this time the mushrooms are not connected to the crown of the cylinder (see also figure 4e). However, the mushrooms do not 'move away from the cylinder in the direction of its oscillation', as imagined by Honji (1981). In fact, the tubes of contra-rotating vortices come closer to the cylinder. Observations of video tapes show qualitatively that the rate of rotation of vortices decreases. This may be partly due to the cut-off of a new supply of vorticity, partly due to the diffusion of vorticity of the vortices (mostly along the tube, as evidenced by the intensification of the dye along the crown of the streak), partly due to the annihilation of vorticity in the overlapping regions of the contra-sign vortices, and partly due to the relaxing (as opposed to stretching) of the vortex tubes. This results in a decrease of the mutual induction velocity of the vortices (and their images) and the distance between the vortex centres increases slightly due to the increase of the image-induced lateral velocities. At this time, the mushrooms become most receptive to the infusion of new boundary-layer fluid. As the velocity of the ambient fluid reaches a critical value (at about $T/8$ every half-cycle), a lump of dyed fluid is thrust forward for a time interval of $\Delta t \approx T/10$ from the boundary in an eruptive manner as seen in the video and figure 4(b). The rhythmic ejection of the boundary-layer fluid is completed before the velocity reaches its maximum at $T/4$. Clearly, the infusion of dye into the mushroom is not a continuous process (this is where the power of video is most welcome). Its clock-like regularity is indeed fascinating to observe. The start of the eruption is accompanied by the dividing into two blobs of the previously ejected fluid, now near the crown of the mushroom. Figure 4(c) shows that the injected dye started moving up the stem towards the mushroom. Figure 4(d) depicts the time at which the stems are beginning to loose their identity and the mushrooms are just beginning to expand laterally. Finally, the stems become completely devoid of dye, as seen in figure 4(e), and shortly thereafter the mushrooms return to their state shown in figure 4(a). It appears that there is an intricate phase relationship between the occurrence of various elements of the characteristic events (maximum

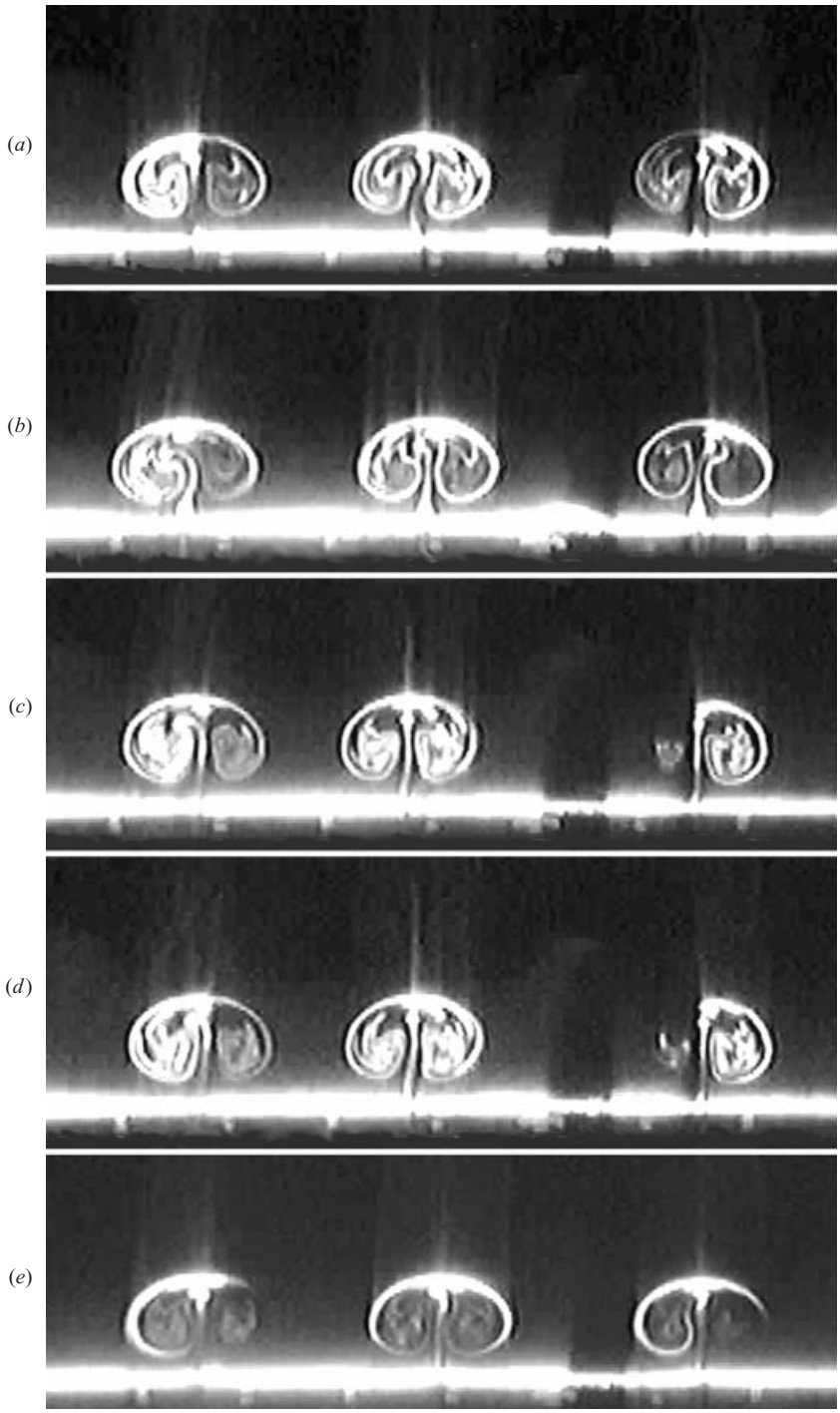

FIGURE 4. Successive frames show how the size and position of a mushroom are sustained through the periodic injection of fresh momentum. When the injected dye almost reaches the crown of the mushroom, it is divided into two parts, one captured by one of the vortices and the other by its contra-rotating companion. The injection and stretching energize the vortices periodically and maintain the size and position of the mushrooms more or less steady. Other details as figure 3.

velocity, maximum receptivity of the mushroom to new injection, the dividing of the injected fiuid into two blobs) which helps to synchronize the feeding mechanism.

It appears that the boundary-layer fluid is provided to the mushrooms in finite quantities each time the velocity of the ambient flow reaches about $0.5U_m$. The details of flow within the ejected lump cannot be seen. However, it appears that it transports sufficient momentum into the mushroom from the region where the two lateral boundary layers collide. Partial evidence is also provided by the regular breakup of the lump into two parts (always and only two parts) as soon as it reaches the top of the mushroom. One part rolls off to the right and the other part (not necessarily half) rolls off to the left. Observations show that the contra-rotating vortices of the mushroom quickly energize and increase their rate of rotation. It appears that the incremental infusion of mass and momentum into the mushrooms, the impulse imparted to the contra-rotating vortices at times when the ambient velocity reaches about 50% of its maximum, and the stretching of the vortices are the mechanisms which sustain the mushrooms and the 'tubes' as long as the mushrooms maintain a quasi-stable arrangement. The mechanism of periodic infusion of dye (boundary-layer fluid) into the mushrooms occurs only at $K = K_h$. In other words, it is unique to the fully grown mushrooms which are sustained by the prevailing flow conditions at an appropriate threshold of Ta. It does not occur in the region $K_{cr} < K < K_h$.

The mushrooms do not remain indefinitely in a quasi-stable state. There appear to be some fundamental reasons for this: the unequal impulse imparted to the left- and right-hand vortices in the mushroom (thought to be the cause of mushroom asymmetry noted in connection with figure 3) and the instability of an ideal arrangement of nearly symmetric contra-rotating vortices and their images, which lead to mushroom merging, creation of new mushrooms, or mushroom breakdown.

3.1.2. *Merging of the mushrooms*

It is already apparent from the foregoing that mushrooms are not perfectly stable structures even at $K = K_h$ and there is considerable interaction between them on either side of the Hall line. This will be illustrated here only at one K_h value even though it occurred at all K and β values leading to mushrooms.

Figure 5(a) shows three mushrooms. They are more or less, but not exactly, identical, as is often the case with all other mushrooms. We will now describe the evolution of the interaction between the second and third (from the left) mushrooms and their reduction to a single mushroom through merging. Figure 5(b) shows that this pair approach each other at each $U = 0$ (when no stem is visible as in figure 5b) and separate during the periods of $U = U_m$ as in figure 5(c). This rocking motion continues with the result that the vorticity of the right-hand vortex of the left-hand mushroom and the vorticity of the left-hand vortex of the right-hand mushroom gradually annihilate each other in their overlapping regions (as in figure 5f). Then, a very interesting phenomenon happens. The counter-rotating vortex pair in figure 5(g) is now fed by two stems: the left-hand vortex by the left-hand stem and the right-hand vortex by the right-hand stem. This event continues for several more cycles, as seen in figures 5(h) and 5(k), and then there is only one stem and one mushroom as seen in figures 5(n) and 5(p) during the periods of maximum velocity. It is also apparent that the first mushroom remained largely unaffected by the merging of the neighbouring pair.

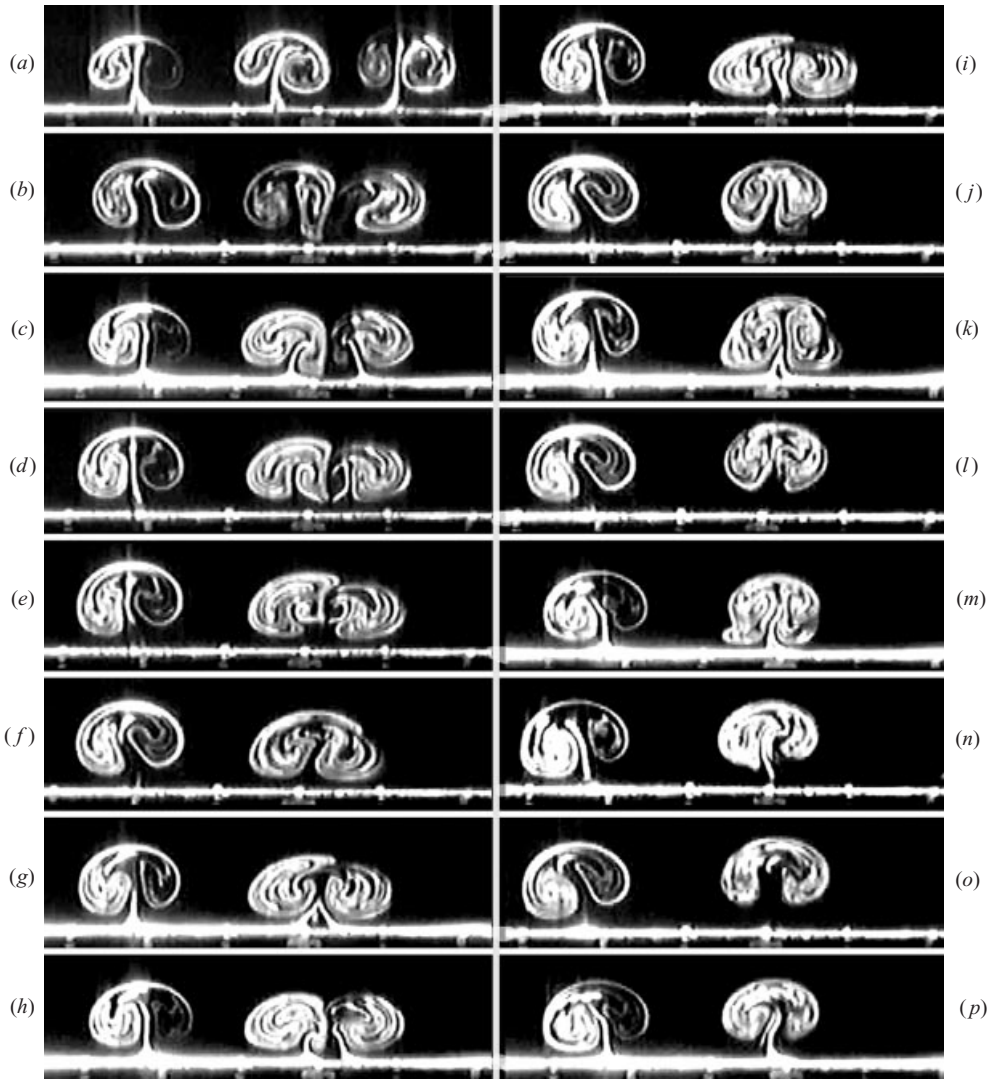

FIGURE 5. Even the perfect mushrooms merge: the evolution of this merging is shown in this figure. It is particularly interesting that the two stems feeding the mushrooms (frames g, h) finally become one (p) when the merging is complete. Other details as figure 3.

3.1.3. *Representative mushrooms for K_h at larger β values*

There is a consistent reduction in the scales (size and spacing) and a notable increase in the mutual interaction of mushrooms with increasing β. The closer they are, the stronger the interaction. Furthermore, their shape, orientation and symmetry are not as uniform as in, for example, figures 4. Figure 6 shows representative mushrooms recorded during part of a single cycle (at 32 ms intervals). Observations have shown that the structures, regardless of the number of cycles, do not necessarily acquire the same size and shape at the same time. Some grow larger and others grow to the same size at a later time. This, once again, reinforces the point noted earlier that the mushrooms are inherently unstable even on the Hall line and that the instability increases with increasing β. Figure 7 corresponds to the point $(0.169, 1.365 \times 10^6)$ on

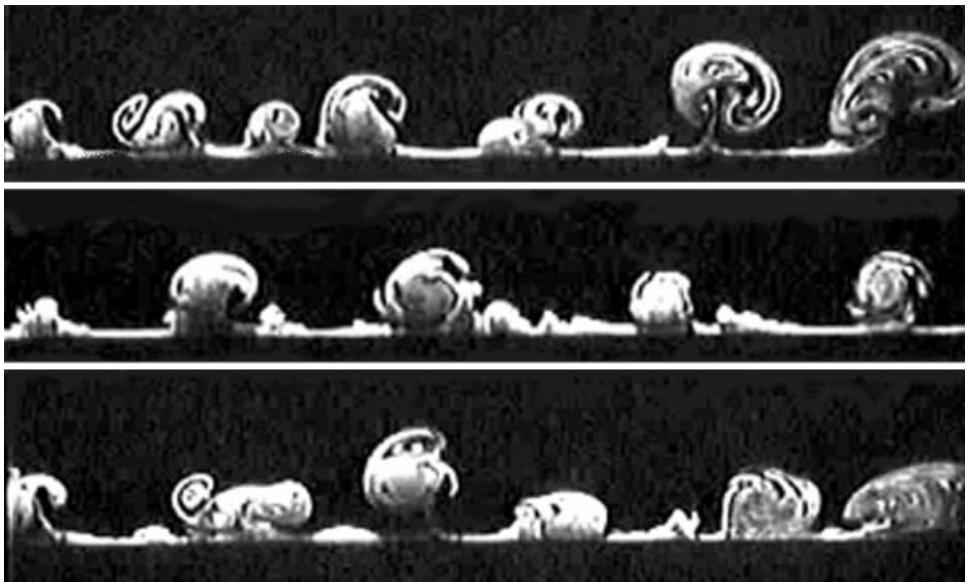

FIGURE 6. Representative mushrooms recorded during part of a single cycle (at 32 ms intervals). The structures, regardless of the number of cycles, do not necessarily acquire the same size and shape at the same time. Some grow larger and others grow to the same size at a later time. This reinforces the notion that the mushrooms are inherently unstable even on the H line. Third facility, $A = 19.8$ mm, $D = 355.6$ mm, $f = 0.623$ Hz, $K = 0.35$, $\beta = 7.4 \times 10^4$, $s/D = 0.008$.

H (see figure 2), which is more appropriate than Honji's (1981) data ($68.8 < \beta < 700$) for comparison with Hall's (1984) analysis by virtue of its assumption of large β. The characteristic features of the mushroom-shaped structures are apparent, but they are far from regular. The average relative spacing between them (over twenty cycles of observations, beyond the initial period of establishment) is about $s/D = 0.005$. Some of the mushrooms occasionally rise above the others and then continuously evolve during the cycle. Apparently, the structures at high β are not as regular as those at lower β. This completes the discussion of the representative mushroom-shaped coherent structures on the Hall line in figure 2.

3.2. *Instabilities and quasi-coherent structures*

Each test began at a point defined by (K, β) in figure 2. Experiments were carried out either by maintaining β constant (i.e. the frequency of oscillation) and decreasing K from an initial value of $K > K_{cr}$ down to K values smaller than K_{cr}, or by maintaining K constant and increasing β (i.e. the frequency f). Each change in either K or β is followed by a long rest and 'refueling' (new dye introduction) period. In the following, the inception of the instabilities near $K = K_{cr}$, the growth and decay of the instabilities in the region $K_{cr} < K < K_h$, larger-scale instabilities in the region $K > K_h$, and, finally, the quantification of the stability boundary and the wavelength s/D are discussed.

3.2.1. *Inception of instabilities and the delineation of* $K = K_{cr}$

The line S (denoting stability) in figure 2 defines the approximate boundary that separates the stable region on the left from the unstable region on the right. It is the lower limit of K for a given β or the lower limit of β for a given K where either no instabilities are created during the entire cycle or those created at $U > 0.5U_m$ barely

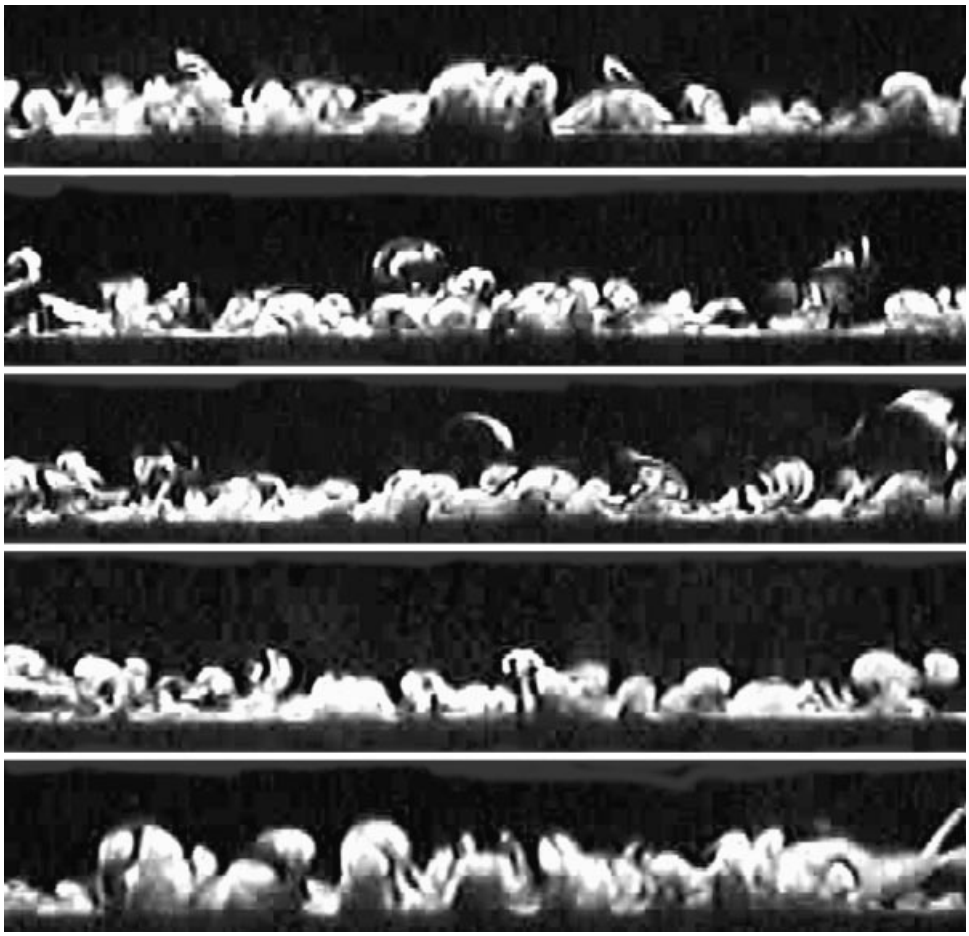

FIGURE 7. These structures are at the highest β achievable in the experiments on the Hall line. The characteristic features of the mushroom-shaped structures are still apparent but not as precise as those of at lower β. Some of the mushrooms occasionally rise above the others and then continuously evolve during the cycle. The average relative spacing between them is based on over twenty cycles of observations. Third facility, $A = 13.3\,\text{mm}$, $D = 495\,\text{mm}$, $f = 5.86\,\text{Hz}$, $K = 0.169$, $\beta = 1.365 \times 10^6$, $s/D = 0.005$.

survive during the period of minimum ambient velocity. Part of the subjectivity, aside from the human interpretation of the definition of the life of a disturbance or QCS, comes from the fact that there cannot be a single line separating the stable region from the unstable region due to the statistical nature of the intermittency of the structures. In fact, the difficulty of the determination of the stability line cannot be adequately emphasized. It depends not only on the parameters that can be controlled but also on those which are, to all intents and purposes, beyond the capacity of the experimenter to control (e.g. temperature gradients, residual background turbulence, very small air bubbles, higher-order harmonics of the vibrations, nonlinear interaction of various types of perturbations, just to imagine a few).

A serious attempt was made to define a line K_l to the left of which no disturbances are observed at any time during at least forty cycles; to define another line, called K_f on which about half (as judged by eye) of the disturbances (created by high velocities) survived the period of maximum acceleration, and finally, to define a line

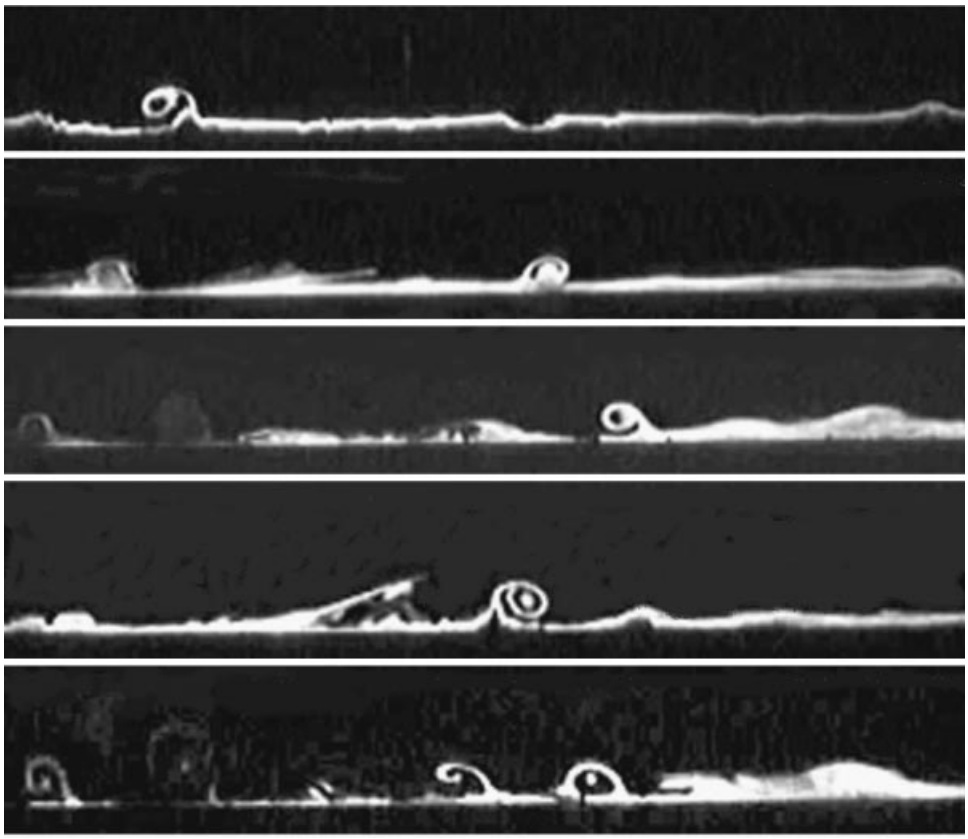

FIGURE 8. The evolution of wave crests and streamwise vertical structures is shown as samples from different runs as U approaches U_m. These disappear quickly as U decreases to 0. Except for the position and direction of the streamwise single vertical structures, the flow state repeats indefinitely. Third facility, $A = 6.8$ mm, $D = 355.6$ mm, $f = 1$ Hz, $K = 0.098$, $\beta = 1.2 \times 10^5$.

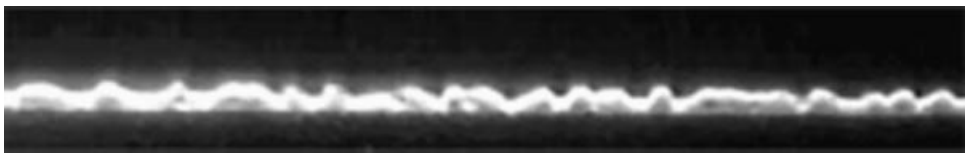

FIGURE 9. The crests of a large number of waves spanning the width of the light sheet are shown at $U = U_m$ for $K = 0.045$ and $\beta = 1.365 \times 10^6$ (a point slightly to the right of S). They disappear as U approaches zero. The appearance of these waves and the growth of structures from their crests are entirely consistent with the centrifugal nature of the instability leading to coherent structures on the Hall line. Third facility, $A = 3.4$ mm, $D = 495$ mm, $f = 5.86$ Hz, $K = 0.045$, $\beta = 1.365 \times 10^6$.

K_g on which the disturbances existed at all times, even though not at the same apparent size during the periods of maximum and minimum velocity. This effort turned out to be extremely complex and not deterministic enough in view of the scatter in the data. It was eventually decided to reduce the boundary to a marginal or fuzzy region, represented by an average line S or the relationship K_{cr}–β.

First, it is necessary to describe the nature of small finite disturbances or the smallest observable structures that appear only during the periods of high ambient velocity (U larger than about $0.5U_m$). The structures always grow at a wave crest.

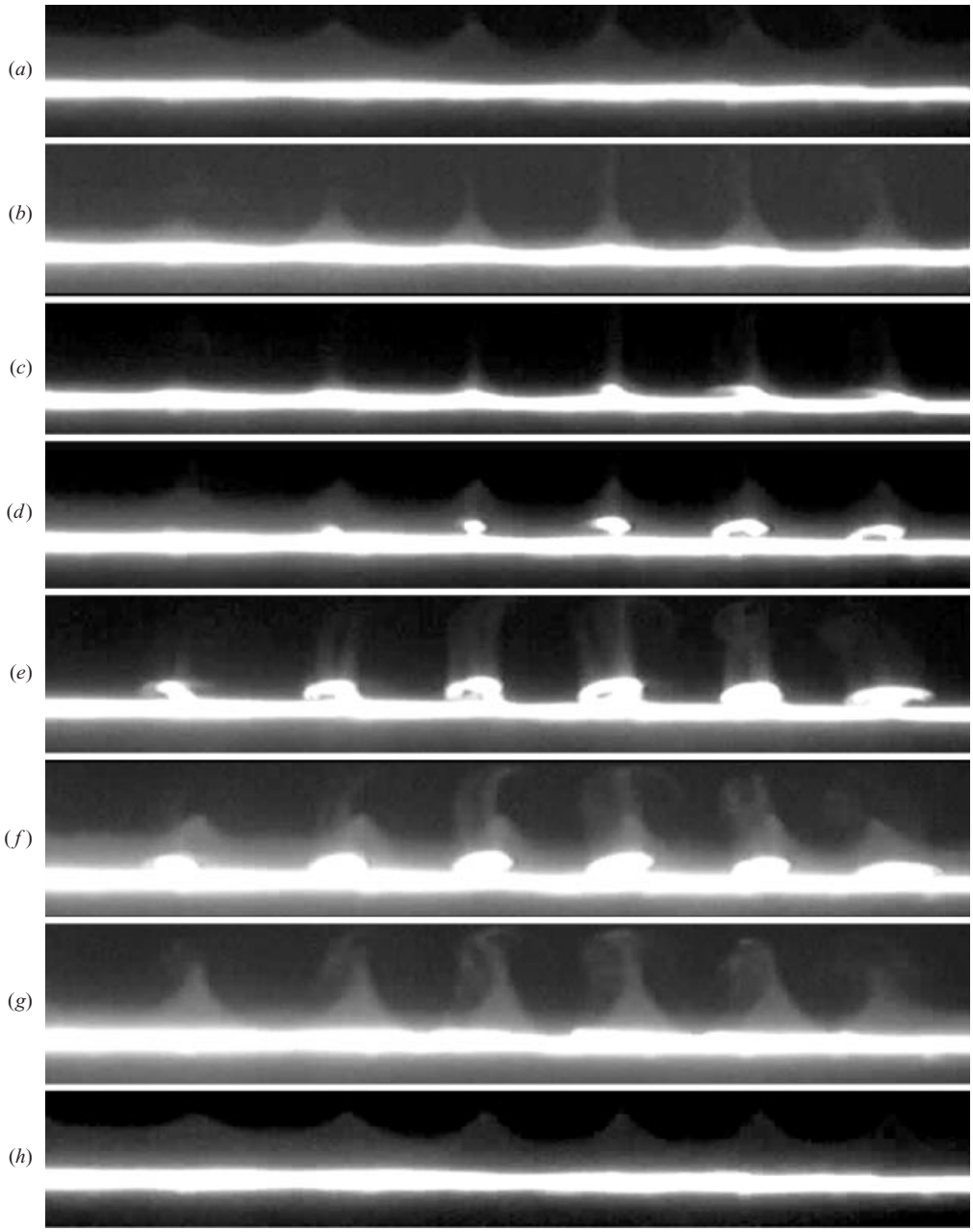

FIGURE 10. The evolution of disturbances at a smaller Stokes number shows that first the wave crests appear as the velocity begins to increase, and then the small structures grow, on some or on all of the crests. Then they begin to decay and rapidly disappear as the velocity approaches zero. This cycle continues indefinitely, with minor variations in the shapes of the structures. First facility, $A = 9.6\,\text{mm}$, $D = 171.6\,\text{mm}$, $f = 0.187\,\text{Hz}$, $K = 0.443$, $\beta = 5221$.

The number of crests along the wave spanning the crown of the cylinder depends on K and β. For a wave with multiple crests, the wavelength decreases with increasing β for a given K. Figure 8 shows the evolution of wave crests and streamwise vortical structures for $K = 0.098$ and $\beta = 1.2 \times 10^5$ (a point slightly to the left of S on

figure 2). As noted earlier, these disappear quickly as $U \to 0$. Figure 9 shows the crests of a large number of waves spanning the light sheet as U approaches U_m for $K = 0.045$ and $\beta = 1.365 \times 10^6$ (a point slightly to the right of S). These too disappear as U approaches zero. Finally, figure 10 shows the evolution of the instability for $K = 0.443$ and $\beta = 5221$. First the wave crests appear as the velocity begins to increase, as in figure 9, and then the small structures grow, on some or on all of the crests (figure 10c). The structures continue to grow, as in figure 10(d, e), then begin to decay, as in figure 10(f, g), and finally completely disappear, as in figures 10(a) and 10(h), as the velocity goes through zero. This cycle continues indefinitely, with minor variations in the shapes of the structures, as long as K and β are maintained constant. The appearance of waves and the growth of structures from their crests are entirely consistent with the centrifugal nature of the instability, eventually leading to coherent structures on the Hall line.

The foregoing represents only a few examples used in the delineation of the stability line. Many more experiments were carried out in the range of $10^3 < \beta < 1.4 \times 10^6$, including those during which no structures were created at any period of the flow regardless of the cycles of oscillations. These observations were particularly significant in demonstrating the fact that there is indeed a stable region in which no disturbances, either due to Taylor–Görtler instability or boundary-layer type instability, can temporally grow to finite amplitude at any time and in any cycle regardless of the number of cycles (minimum 50 cycles).

3.2.2. *Instabilities in the region $K_{cr} < K < K_h$*

Only the most representative figures showing the character of the quasi-coherent structures will be presented. The structures between the S and H lines grow and diminish in size during the periods of high and low velocity. Figure 11 shows the sequential (but not at equal time intervals) evolution of the structures in a given cycle between the two instances of $U = 0$. The mushroom-like structures grow in size and number as the velocity increases. Then they begin to diminish and return to a state not very far from, but not identical to, the first frame (figure 11a). Figure 12 shows, at a larger K and β, representative structures (at different times in a cycle) which are very similar to those encountered in oscillating flow about plates (Sarpkaya 1993). Finally, figure 13 shows the sequence of flow structures at $U = 0$, $U = U_m/2$, and $U = U_m$ for a much larger β.

The primary characteristics of the structures between the S and H lines for a given β are that for K closer to K_{cr}, the structures strongly evolve during a given cycle and rarely return to the same shape and position they had at the start of the cycle. As K increases towards K_h, they become more regular (like small mushrooms) and increase in size and number. Thus, there is a continuous, but complex, evolution of structures from a transverse wave, on or about the S line, to a series of highly regular mushrooms on the Hall line. However, even on the Hall line the mushrooms are subject to mutual interactions.

In the light of the foregoing, it appears that the threshold value of the Taylor number found by Hall (1984) corresponds only to points on the H line where the mushrooms can sustain themselves in the manner described earlier. When the centrifugal force at $U = U_m$ is large enough to give rise to structures (not necessarily mushroom-shaped) but not large enough to trigger a feeding mechanism to fully sustain them near $U = 0$, the structures become quasi-coherent, with ever changing sizes and shapes. Representative examples of these have been presented above. It

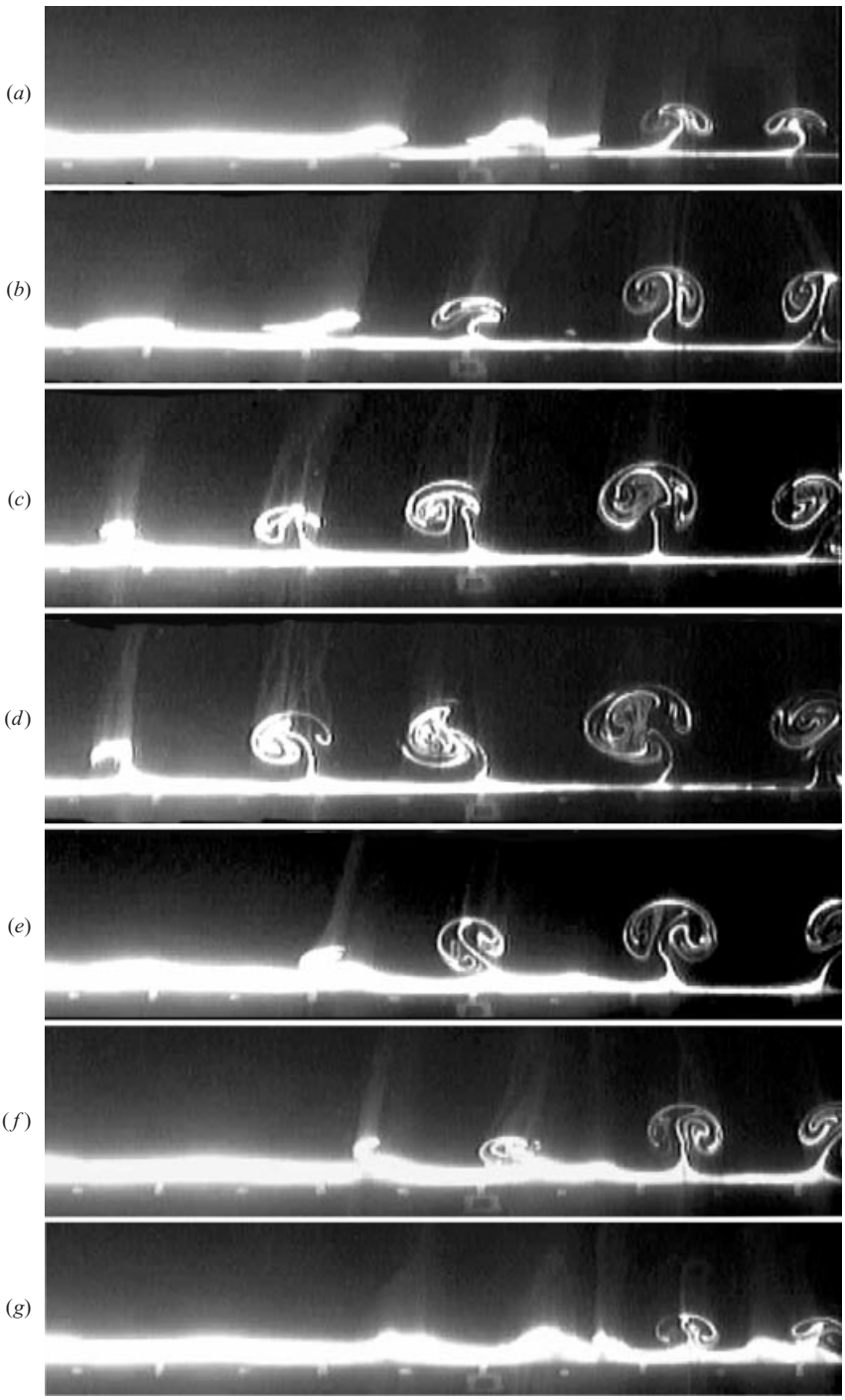

FIGURE 11. Photographs show in sequence (but not at equal time intervals) the evolution of the structures in a given cycle, starting at $U = 0$. The mushroom-like structures grow in size and number as the velocity increases. Then they begin to diminish and return to a state not too far from the first frame. First facility, $A = 13.7$ mm, $D = 171.6$ mm, $f = 0.187$ Hz, $K = 0.50$, $\beta = 5221$.

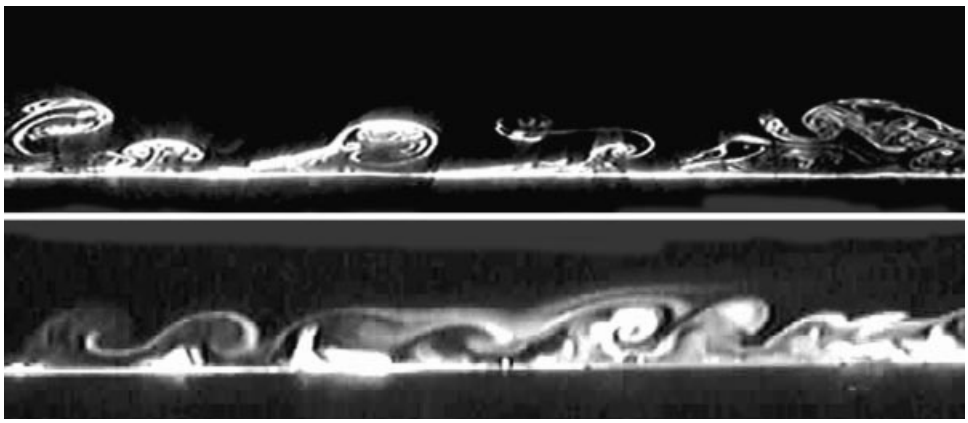

FIGURE 12. The two photographs show at $U = U_m$ two highly distorted mushroom-like structures which are very similar to those encountered in oscillating flow about plates. They eventually transform into regular mushrooms as K increases to about 0.6. Second facility, $D = 152.4$ mm, $f = 0.45$ Hz, $\beta = 9956$: (*a*) $A = 10.2$ mm, $K = 0.42$; (*b*) $A = 8$ mm, $K = 0.33$.

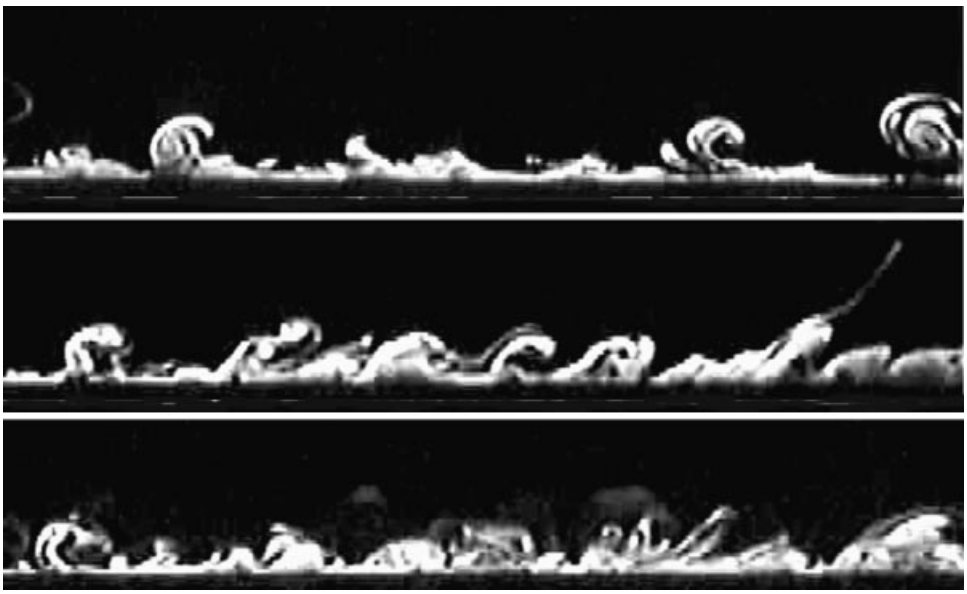

FIGURE 13. The evolution of structures at a larger Stokes number at (*a*) $U = 0$, (*b*) $U = U_m/2$ and (*c*) $U = U_m$ in a half-cycle. Third facility, $A = 11$ mm, $D = 495$ mm, $f = 3.21$ Hz, $K = 0.14$, $\beta = 7.48 \times 10^5$.

appears that an analysis of the transient growth signature of the centrifugal instability is needed to theoretically delineate the region between the S and H lines.

3.2.3. *Instabilities in the region $K > K_h$*

In the region to the right of H one encounters, with increasing K, first mushroom-shaped structures, then quasi-coherent structures, and eventually, chaotic motion, and if K is large enough, turbulence and separation. The experiments reported here are confined to $K < 0.8$.

Figure 14 shows, for $\beta = 3 \times 10^4$, how rapidly the structures change even though

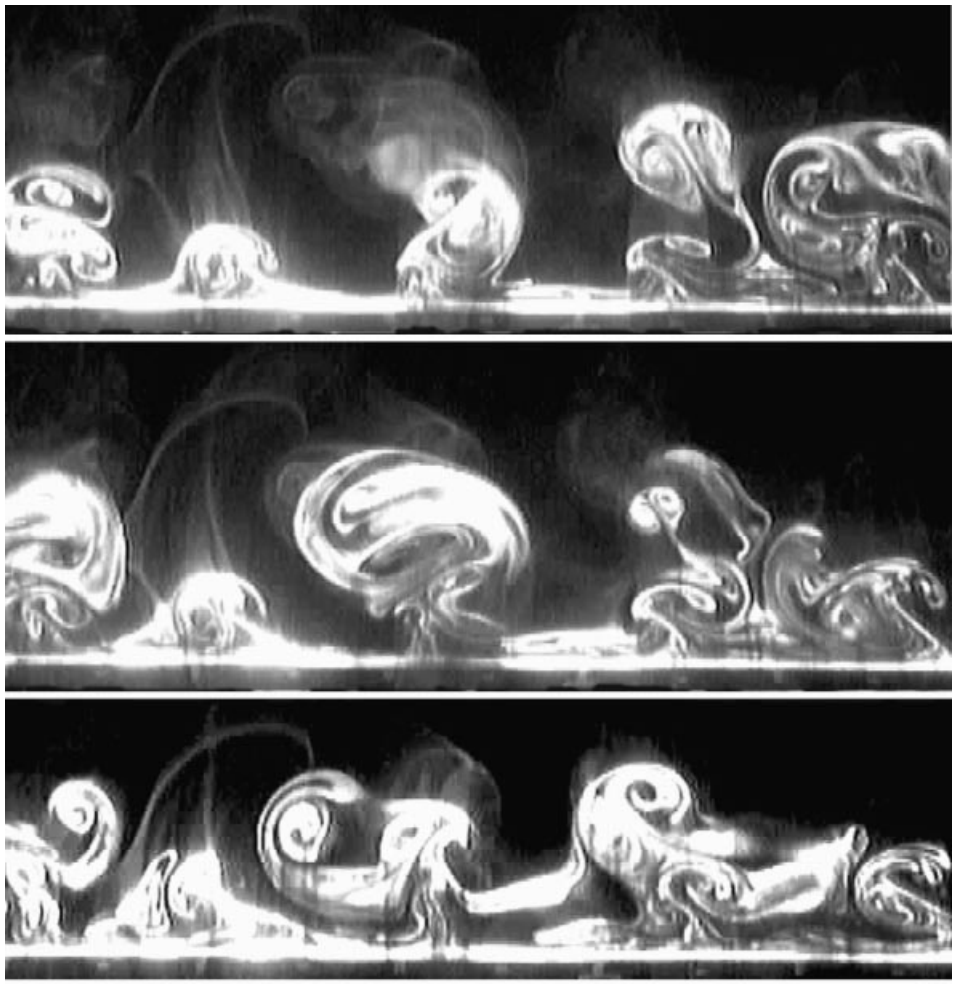

FIGURE 14. A sequence showing the rapid interaction between the structures and the vortex tubes on the right-hand side of the Hall line (they are only 3 ms apart). Second facility, $A = 22.5$ mm, $D = 228$ mm, $f = 0.56$ Hz, $K = 0.62$, $\beta = 3 \times 10^4$.

they are only 3 ms apart. Vortex tubes are identifiable on some of the structures. Figure 15 shows, for $\beta = 1.2 \times 10^5$, the intermingling of the vortex tubes and their extremely rapid wrapping–unwrapping motion during one cycle. Note the striking similarity between the figures 15(*a*) and 15(*e*) and the fact that for the K and β values under consideration the structures rise renewed from the chaotic motion to start another cycle. Eventually, they bear no resemblance to the structures which occurred five or ten cycles back. Finally, figure 16 shows, at $\beta = 1.365 \times 10^6$, the highest β encountered in the experiments, several instants where one can observe parts of one or more highly deformed mushrooms which rapidly change in the subsequent frames.

3.2.4. *Quantification of the stability boundary*

The entire data set obtained in the course of this investigation is shown in figure 17 (a replot of figure 2, but with data). The equation that best represents the line S is

$$K_{cr}\beta^{2/5} = 12.5. \tag{3.1}$$

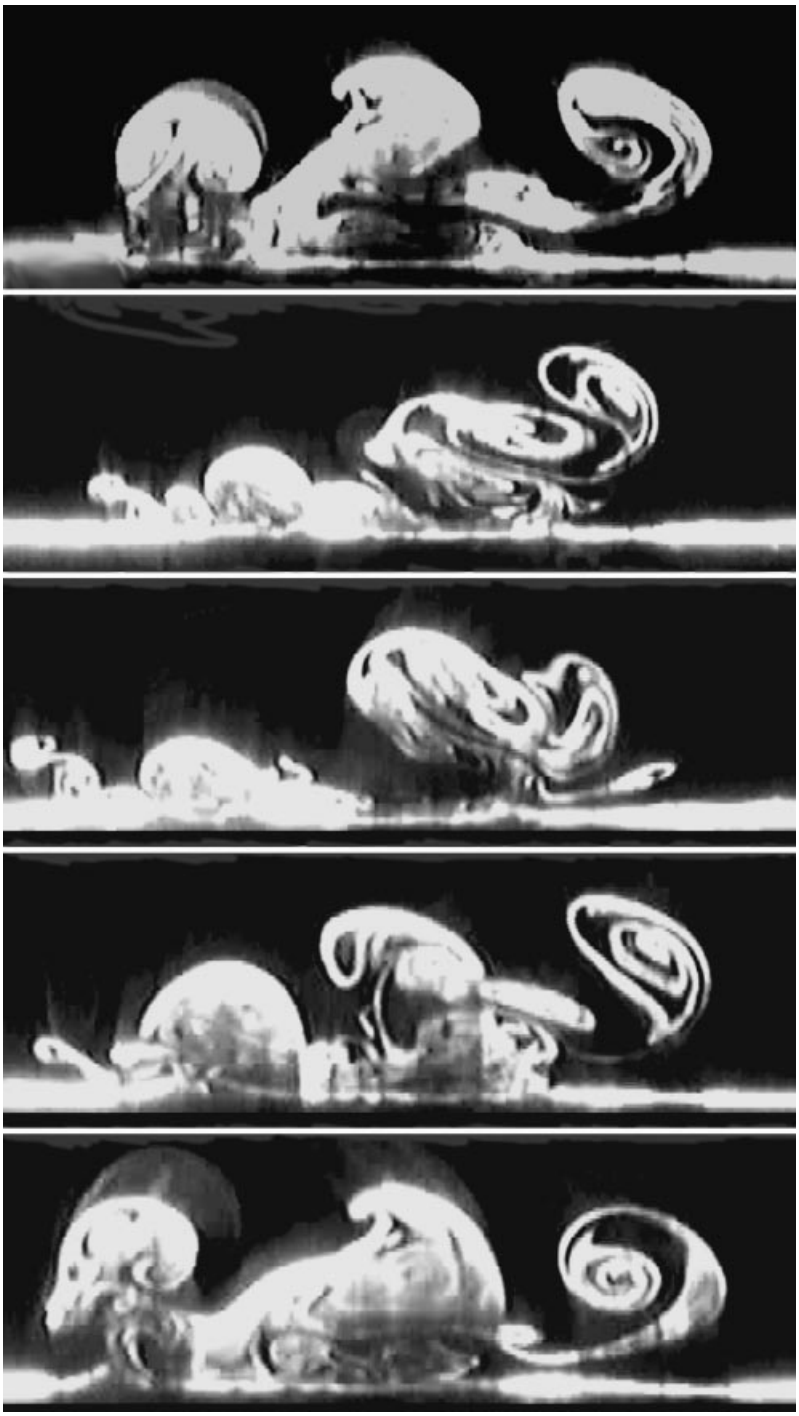

FIGURE 15. A sequence showing how quickly the vortex tubes undergo wrapping and unwrapping around each other during a single cycle. Note the striking similarity between (*a*) and (*e*) and the fact that for the K and β values under consideration the structures recover from a highly chaotic state only to start anew from a nearly identical initial state. Third facility, $A = 29.5\,\text{mm}$, $D = 355.6\,\text{mm}$, $f = 1\,\text{Hz}$, $K = 0.52$, $\beta = 1.2 \times 10^5$.

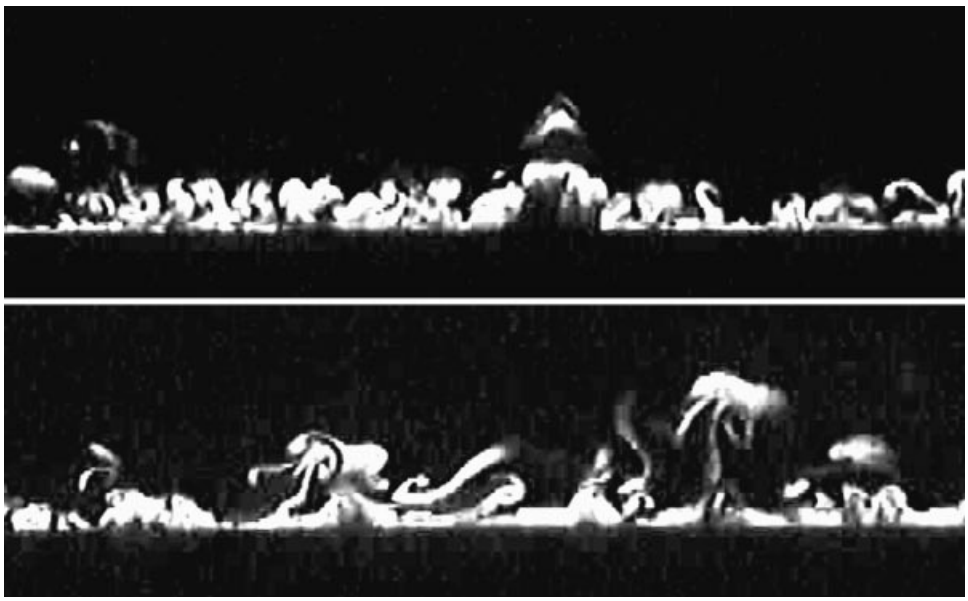

FIGURE 16. Representative photographs show, at the highest β encountered in the experiments, several instants where one can observe parts of one or more highly deformed mushrooms in the region to the right of the Hall line. Third facility, $A = 23.6$ mm, $D = 495$ mm, $f = 5.86$ Hz, $K = 0.3$, $\beta = 1.365 \times 10^6$.

The line H is, as noted earlier, represented to a first order of approximation by

$$K_h \beta^{1/4} = 5.78. \tag{3.2}$$

The Reynolds number along the stability line increases as $Re = 12.5\beta^{3/5}$. It rises from 300 at $\beta = 200$ to about 50 000 at $\beta = 10^6$.

In the light of the foregoing, brief comments will be made regarding the previous works. Sarpkaya (1986), using a sinusoidally oscillating flow about a smooth cylinder, found that the onset of the instability spans the interval $K = 0.6$ to 0.82 for $\beta = 1035$. This is close to $K_{cr} = 0.78$ at $\beta = 1035$. Similarly, for $\beta = 1380$ ($K_{cr} = 0.69$) experiments exhibited a region of hysteresis as K was increased in small steps from 0.4 to about 1. $K_{cr} = 0.69$ corresponds to the first deviation from the maximum of the first rise in the drag coefficient above the Stokes (1851)–Wang (1968) line (see figure 2 in Sarpkaya 1986). Furthermore, the nature of the instability due to its sensitivity to disturbances is such that the occurrence of a region of hysteresis is not entirely unexpected. Honji (1981) observed, in connection with his figure 3 ($K = 1.16$ and $\beta = 599$), that the separated dye sheet is 'slightly distorted wavily'. This particular data point at a K value slightly smaller than K_h ($= 1.218$ for $\beta = 599$) is shown in figure 17, and, according to our stability line, one should indeed expect to see the type of 'wavy' instability observed by Honji. It is also clear that within the range of the β values used by Honji ($68.8 < \beta < 700$), near the intersection of the S and H lines, Honji could not have seen enough quasi-coherent structures, except as noted above. The wavelength of the instability observed by Honji is approximated from his figure 3 as $s/D = (1.95\,\text{mm}/37.7\,\text{mm}) = 0.52$.

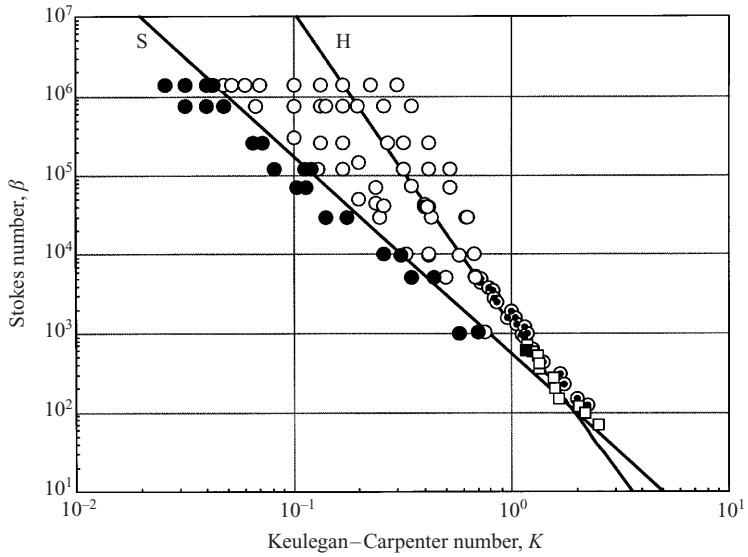

FIGURE 17. The stability zones and the data obtained in the course of the investigation: the region to the left of line S is stable. A narrow region on either side of the S line is marginally stable. The region between the marginally stable state and the Hall line is unstable. The Hall line (Hall 1984) is where nearly perfect mushrooms occur. The symbols between the S and H lines denote instability in the form of quasi-coherent structures, the symbols on the H line denote mushroom-type coherent structures: ● (stable), ○ (unstable), present data; ⊙, Sarpkaya (1986); □ and ■ ($K = 1.16$ and $\beta = 599$), Honji (1981). On the right of the Hall line the mushroom-shaped structures eventually become chaotic with increasing K.

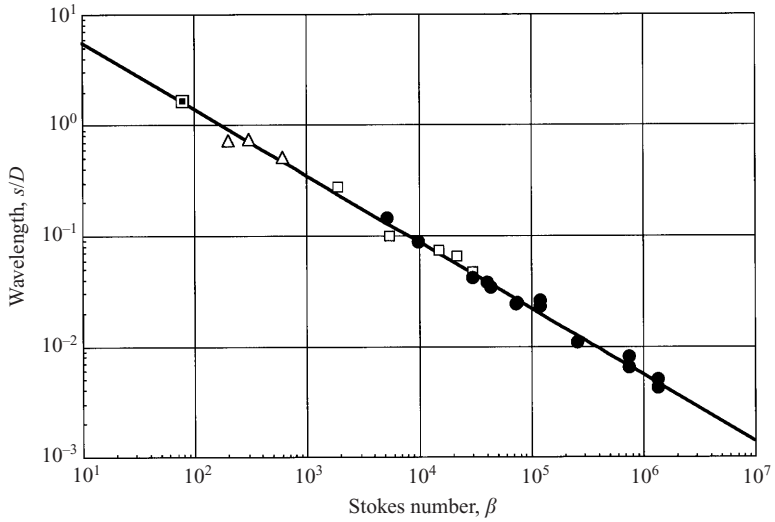

FIGURE 18. Measurements of the wavelength of the mushroom-type coherent structures versus β. ●, present study; □, Bearman & Mackwood (1992); ▣, Tatsuno & Bearman (1990); △, Honji (1981).

3.2.5. *Quantification of the mushroom spacing*

The wavelength s/D of the mushroom-shaped coherent structures is shown in figure 18. As it was increasingly difficult to quantify s/D at higher β values, the data for β larger than about 10^5 represent the averages of several measurements by two

independent workers. An empirical relationship of the form

$$\frac{s}{D}\beta^{3/5} = 22 \tag{3.3}$$

represents the mean line through the data within the range of β values encountered. It suggests that the structures at much larger β values of industrial significance will indeed be extremely close together, leading to intense interaction between myriads of vortex tubes with their contra-rotating vortices. The state of such a flow and what it might do to the shear stresses on the boundary can only be imagined.

4. Concluding remarks

Experiments in three different facilities through the use of flow visualization have clarified the nature of the small-amplitude oscillatory flow over smooth circular cylinders. The most interesting result has been the discovery of two related facts: the flow to the left of the Hall line is not stable, and a fully grown mushroom is not the only form of instability. There is a stable region to the left of S in which no discernible flow structures occur near the crown of the cylinder during any part of the oscillation cycle. There is an unstable region between S and H where many forms of quasi-coherent structures occur (for β larger than about 100). There is a marginal-stability region between the stable and unstable regions in which small structures appear and disappear as the ambient velocity goes from maximum to zero. On the Hall line, structures take the form of mushrooms even at the highest β encountered in these experiments. In the light of the extensive observations, it appears that the threshold value of the Taylor number found by Hall (1984) corresponds only to points on the H line where the mushrooms can sustain themselves through a rhythmic feeding of the boundary layer fluid. When the centrifugal force at $U = U_m$ is large enough to give rise to structures (not necessarily mushroom-shaped) but not large enough to trigger a rhythmic feeding mechanism to fully sustain them near $U = 0$, the structures acquire myriads of quasi-coherent forms, with ever changing sizes and shapes, some of which are reminiscent of the quasi-coherent structures in steady flow over flat walls.

To the right of the Hall line, instabilities take many forms and, with increasing K, fall under the influence of turbulence and separation and all of their attendant consequences (currently under investigation).

The tracking and quantification of coherent and quasi-coherent structures at any point in the (K, β)-plane through the use of direct numerical simulations might help in understanding the many fascinating characteristics of the mushroom-type coherent structures and the existence of an unstable region composed of quasi-coherent structures.

An effort was made to measure the drag of circular cylinders (smooth, rough) subjected to sinusoidally oscillating motion, particularly at large values of β, to gain some insight into the magnitude of their damping and, in particular, into the relationship between the deviation of the measured drag values from the Stokes–Wang stable laminar flow solution (see e.g. Sarpkaya 1986) and the instability of the flow under discussion. The experiments, confined to one relative roughness ($k/D = 0.01$ where k is the mean roughness height of sieved sand), revealed no stable region for the K and β values encountered in our experiments. These are not described here in detail because more extensive experiments are now underway with smaller roughness elements, at smaller K values. These and the effect of coherent and quasi-coherent

structures on the hydrodynamic damping of compliant systems will be the subject of a future publication.

This work began in 1993 in connection with a special programme on the stability of periodic flows supported by the National Science Foundation, Office of Naval Research, and the Naval Postgraduate School. This support is gratefully acknowledged. The constructive comments of the reviewers are sincerely appreciated. Finally, a special thanks are extended to Mr Phil Parker, for his assistance with the experiments.

REFERENCES

Batchelor, G. K. 1967 *An Introduction to Fluid Dynamics*. Cambridge University Press.

Bearman, P. W. & Mackwood, P. R. 1992 Measurements of the hydrodynamic damping of oscillating cylinders. In *Proc. 6th Intl Conf. on the Behavior of Offshore Structures* (*Boss '92*), London, pp. 405–414.

Gershuni, G. Z. & Lyubinov, D. V. 1988 *Thermal Vibrational Connection*. John Wiley & Sons.

Hall, P. 1984 On the stability of unsteady boundary layer on a cylinder oscillating transversely in a viscous fluid. *J. Fluid Mech.* **146**, 337–367.

Hara, T. & Mei, C. C. 1990*a* Oscillating flow over periodic ripples. *J. Fluid Mech.* **211**, 183–209.

Hara, T. & Mei, C. C. 1990*b* Centrifugal instability of an oscillatory flow periodic ripples. *J. Fluid Mech.* **217**, 1–32.

Honji, H. 1981 Streaked flow around on oscillating circular cylinder. *J. Fluid Mech.* **107**, 507–520.

Koga, D. J., Abrahamson, S. D. & Eaton, J. K. 1987 Development of a portable laser sheet. *Exps. Fluids* **5**, 215–216.

Lyne, W. H. 1971 Unsteady viscous flow over a wavy wall. *J. Fluid Mech.* **50**, 33–48.

Probstein, R. F. 1995 *Physicochemical Hydrodynamics*. John Wiley & Sons.

Sarpkaya, T. 1976 Vortex shedding and resistance in harmonic flow about smooth and rough circular cylinders. *Proc. First Intl Conf. Behavior of Offshore Structures* (*BOSS '76*), *The Norwegian Institute of Technology*, Vol. 1, pp. 220–235.

Sarpkaya, T. 1977 In-line and transverse forces on cylinders in oscillatory flow at high Reynolds numbers. *J. Ship Res.* **21**, 200–216.

Sarpkaya, T. 1986 Force on a circular cylinder in viscous oscillatory flow at low Keulegan-Carpenter numbers. *J. Fluid Mech.* **165**, 61–71.

Sarpkaya, T. 1993 Coherent structures in oscillatory boundary layers. *J. Fluid Mech.* **253**, 105–140.

Scandura, P., Vittori, G. & Blondeaux, P. 2000 Three-dimensional oscillatory flow over steep ripples. *J. Fluid Mech.* **412**, 355–378.

Schlichting, H. 1932 Berechnung ebner periodisher Grenzschichtstromungen. *Phys. Z.* **33**, 327.

Schlichting, H. 1979 *Boundary Layer Theory*, 7th edn. McGraw-Hill.

Stokes, G. G. 1851 On the effect of the internal friction of fluids on the motion of pendulums. *Trans. Camb. Phil. Soc.* **9**, 8–106.

Tatsuno, M. & Bearman, P. 1990 A visual study of the flow around an oscillating circular cylinder at low Keulegan-Carpenter numbers and low Stokes numbers. *J. Fluid Mech.* **211**, 157–182.

Volfson, D. & Vinals, J. 2001 Flow induced by a randomly vibrating boundary. *J. Fluid Mech.* **432**, 387–408.

Wang, C.-Y. 1968 On the high frequency oscillating viscous flows. *J. Fluid Mech.* **32**, 55–68.